Catalysis Science & Technology

PAPER

View Article Online
View Journal

CrossMark click for updates

Cite this: DOI: 10.1039/c5cy01712b

La-modified mesoporous Mg–Al mixed oxides: effective and stable base catalysts for the synthesis of dimethyl carbonate from methyl carbamate and methanol†

Dengfeng Wang,[a] Xuelan Zhang,*[ab] Jie Ma,*[a] Haiwen Yu,[a] Jingzhu Shen[a] and Wei Wei[b]

Received 8th October 2015,
Accepted 30th October 2015

DOI: 10.1039/c5cy01712b

www.rsc.org/catalysis

A series of La-containing Mg–Al hydrotalcite-like (HTl) precursors with different La contents (Mg^{2+} : Al^{3+} : La^{3+} = 3 : 1 : *x*, where *x* varies from 0 to 1.0) were synthesized using a co-precipitation method followed by hydrothermal treatment. X-ray diffraction and thermogravimetric measurements demonstrated that the yield of the HTl phase decreased with increasing La content. The La-modified Mg–Al mixed oxides (HTC-La) were then obtained by thermal decomposition of the corresponding HTl precursors, and the mesoporous structure was formed during calcination. It was demonstrated that the structure and surface basic properties of the HTC-La samples strongly depended on the amount of La additive. Simultaneously, the resulting HTC-La materials were used as solid base catalysts for the synthesis of dimethyl carbonate (DMC) from methyl carbamate (MC) and methanol. Then, the correlation between their basic properties and catalytic performance was studied in detail. The incorporation of a suitable amount of La into HTC-La catalysts was beneficial for the production of DMC, and a DMC yield of 54.3% with a high DMC selectivity of 80.9% could be achieved when *x* was tuned to 0.5 under the optimized reaction conditions. In addition, the HTC-La catalyst could be readily recycled while maintaining high catalytic activity and selectivity for DMC. Furthermore, *in situ* FTIR experiments were carried out to elucidate the adsorption behaviours of the reactants. On the basis of the experimental results, a plausible basic catalytic mechanism wherein MC and methanol were activated simultaneously on the basic sites of the catalyst was proposed for this catalytic reaction.

1. Introduction

Recently, much effort has been devoted to the development of new synthesis methods based on CO_2 as a feedstock for organic carbonates owing to their excellent properties and commercial applications. As an important homologue of the dialkyl carbonate family, dimethyl carbonate (DMC) has received much attention. As an environmentally benign building block, DMC can replace phosgene, dimethyl sulphate, chloromethane, and methyl chloroformate as a carbonylation, methylation, esterification, or ester interchange reagent for organic synthesis without pollution. DMC is also used as a green solvent and flavoring agent of foodstuff due to its low toxicity. More important, it is extensively applied as an oxygen-containing fuel additive in place of toxic and less biodegradable MTBE additives. Moreover, DMC has been used as an electrolyte due to its high dielectric constant.[1–4] Up to now, a number of synthetic processes are known for the production of DMC including phosgenation of methanol, oxidation/carbonation of methanol, and transesterification of organic carbonates. However, each of the aforementioned processes suffers from the corresponding shortcomings such as being poisonous, being easily explosive, and having high investment and production costs.[5–7] Recently, CO_2, a readily available, inexpensive and environmentally acceptable material, has been used as a raw material for DMC synthesis. Nevertheless, the direct synthesis of DMC from CO_2 and methanol is still far from practical application because of the difficulty in activation of carbon dioxide, reactivation of the catalyst and thermodynamic limitation.[8–10] In order to overcome these shortcomings, an alternative approach is to prepare DMC from urea and methanol, which is widely considered as an indirect route for utilization of CO_2 because the

[a] College of Chemistry, Chemical Engineering and Materials Science, Zaozhuang University, Zaozhuang, 277160, PR China. E-mail: bitwdf@163.com
[b] State Key Laboratory of Coal Conversion, Institute of Coal Chemistry, Chinese Academy of Sciences, Taiyuan, 030001, PR China

† Electronic supplementary information (ESI) available. See DOI: 10.1039/c5cy01712b

released NH_3 can be easily separated, recycled and further utilized to produce urea by reaction with CO_2. Besides, no water is formed during this process.[11] Therefore, the subsequent separation and purification would be simple and the cost could be reduced markedly. It is well known that urea methanolysis is a typical stepwise reaction: urea firstly reacts with methanol to produce the intermediate methyl carbamate (MC), which is further converted to DMC by reaction with methanol. It is generally accepted that the first step is fast and highly selective even without catalysts, but the DMC synthesis from MC and methanol is more difficult.[12,13] Hence, the second reaction is usually considered to be the rate-control step, and dividing this process into two isolated steps would be a more promising method. Therefore, the key to improve the DMC synthesis *via* methanolysis of urea is to develop effective catalysts towards the reaction of MC and methanol.

Several kinds of catalysts including organic tin, inorganic salts, ionic liquids, pure metal oxides and Fe_2O_3 supported catalysts have been tested towards the direct reaction of urea and methanol or its analogues.[14–18] Among them, zinc-containing catalysts such as ZnO, Zn–Ce, Zn–Ca and Zn–Al mixed oxides presented high catalytic activity.[19–22] Especially, ZnO–CeO_2–La_2O_3 could improve DMC synthesis remarkably and give 50.4% DMC yield.[23] However, the main problem associated with zinc-containing catalysts might be the easy leaching of the active component, which has been proved by several researchers. For instance, Zhao *et al.* reported that ZnO was converted to the homogeneous species when it catalyzed urea alcoholysis.[24] An *et al.* discovered that the ZnO phase of the ZnO–PbO catalyst was seriously leached out when it promoted the reaction of ethyl carbamate and ethanol.[25] Recently, Fujita and co-workers further pointed out that synthesis of glycerol carbonate from urea glycerolysis using Zn-containing solid catalysts took place homogeneously but not heterogeneously.[26] With respect to the isolated second reaction, solid bases were tested in a batch reactor, but the DMC yield was below 20%.[12] Our group reported that using $ZnCl_2$ and $LaCl_3$ as catalysts, the DMC yield could reach 33.6% and 53.7%, respectively.[27–29] However, it is well known that catalyst recovery is a great inconvenience for industrial production using homogeneous catalysts. In order to develop heterogeneous catalysts, we have synthesized a Zn–Fe mixed oxide that gave a DMC yield of 30.7%.[30] Unfortunately, it also had a ZnO phase, which might not resist the flushing of the reactants in the continuous reaction, and its catalytic activity was still relatively low. Thus, it is still a challenging task to develop new heterogeneous catalysts exhibiting good performance for the synthesis of DMC from MC and methanol.

Hydrotalcite (HT) or hydrotalcite-like compounds (HTlcs) are layered double hydroxides belonging to anionic clay with the general formula $[M_{(1-x)}^{2+}M_x^{3+}(OH)_2]^{x+}\cdot(A^{n-})_{x/n}\cdot mH_2O$, where M^{2+} and M^{3+} are the divalent and trivalent cations, respectively. Their structure is very similar to that of brucite, in which some of the divalent metal ions (M^{2+} = Mg^{2+}) could be isomorphously substituted by Al^{3+} or other trivalent metal cations, resulting in the formation of positively charged layers, which in turn are charge compensated by the anions (A^{n-}) such as CO_3^{2-} or OH^- present in the interlayer.[31] More important, the mixed oxides obtained by the thermal decomposition of these compounds exhibit homogeneous dispersion of M^{2+} and M^{3+} at the atomic level, high stability against sintering, high surface area and tunable basic properties.[32–34] Therefore, HTlcs with different compositions are among the most investigated catalyst precursors because of the remarkable properties of the final catalysts, which have been used in many reactions such as aldol condensation, Michael addition, transesterification and so on.[35–38] In our previous work, we have reported that Mg–Al mixed oxide catalysts were effective solid base catalysts for the reaction of urea and phenol.[39] Very recently, we have discovered the promotion effect of transition metal on the basicity and activity of calcined hydrotalcite catalysts for diethyl carbonate synthesis.[40] However, the effect of rare earth element doping on the basicity of calcined hydrotalcite catalysts and their catalytic performance in DMC synthesis remains unknown. As part of our continuous research work, here, we wish to show that La-modified Mg–Al mixed oxides (HTC-La) obtained by calcination of the corresponding La-containing hydrotalcite-like (HTl) precursors are efficient solid base catalysts for DMC synthesis from MC and methanol, and the DMC yield could reach 54.3% under optimal reaction conditions. Besides, their activity could be tailored by simple adjustment of the amount of La additive. The correlations between the textural, chemical, structural, and basic properties of the HTC-La catalysts and their catalytic performances in MC methanolysis were investigated. At the same time, the catalytic activities and recyclability of the catalysts were systematically studied. Finally, we proposed a plausible reaction mechanism wherein MC and methanol were simultaneously activated on the surface basic sites of the HTC-La catalysts based on *in situ* FTIR experimental results.

2. Experimental

2.1 Catalyst preparation

La-containing hydrotalcite-like compounds with various $Mg^{2+}:Al^{3+}:La^{3+}$ atomic ratios were synthesized using a co-precipitation method followed by hydrothermal treatment.[41] The $Mg^{2+}:Al^{3+}:La^{3+}$ atomic ratio in the starting solution was kept at $3:1:x$, where x varied from 0 to 1.0. In a typical procedure, two aqueous solutions, a 100 mL solution of Mg^{2+}, Al^{3+}, and La^{3+} nitrates and a 100 mL mixed solution of NaOH and Na_2CO_3 precipitants, were added dropwise to 100 mL of deionized water under vigorous stirring. The addition was performed over 1.0–1.5 h and the pH value was maintained close to 10 by addition of suitable amounts of 2 M NaOH solution. The resulting gel-like slurry was transferred into autoclaves and hydrothermally treated at 80 °C for 24 h. Then, the as-prepared product was collected after being filtered and washed with deionized water until the pH of the

filter liquor became 7.0. Finally, the precipitate was dried at 100 °C for 12 h to obtain HTl precursors.

The as-prepared HTlcs were further calcined in air at 500 °C for 7 h at a heating-up rate of 5 °C min^{-1} to obtain the final mixed oxide catalysts. The synthesized hydrotalcite-like precursors and corresponding mixed oxides were denoted as HT-*N*La before calcination and HTC-*N*La after calcination, respectively, where *N*/10 represented the $La^{3+}:Al^{3+}$ atomic ratio in the starting solution. For comparison, the $La_2O_2CO_3$ catalyst was prepared under the same conditions using $La(NO_3)_3{\cdot}5H_2O$ as the La source and Na_2CO_3 as the precipitant, followed by calcination at 500 °C for 7 h under a CO_2 atmosphere.

2.2 Characterization

Thermogravimetric analysis (TGA) was performed on a NETZSCH STA-409 thermal analyzer under nitrogen (50 mL min^{-1}) with a heating rate of 10 °C min^{-1} from room temperature to 800 °C to study the thermal decomposition behavior of the catalyst precursors. The powder X-ray diffraction (XRD) patterns of the samples were recorded on a Rigaku Miniflex diffractometer using a Cu target with a Ni filter in the 2θ range of 5–80°. Elemental chemical analysis of the samples was performed using inductively coupled plasma-optical (ICP) emission spectroscopy (Thermo iCAP 6300). Nitrogen adsorption–desorption isotherms were obtained at liquid nitrogen temperature, −196 °C, with a Micromeritics ASAP-2020 instrument (Norcross, GA), using static adsorption procedures. The samples were degassed at 200 °C for 5 h prior to the measurement. The BET isotherm and BJH pore size distribution were used to obtain the specific surface area and pore volume, respectively. The morphology of the samples was investigated using a Hitachi S4800 scanning electron microscope (SEM) with an accelerating voltage of 20.00 kV. X-ray photoelectron spectroscopy (XPS) measurements were performed on a Thermo Scientific k-Alpha spectrometer equipped with an Al anode (Al Kα = 1486.6 eV) operating at 72 W and a spot size of 400 μm under ultrahigh vacuum (10^{-7} Pa). The binding energies were calibrated internally for surface charging by adventitious carbon deposit C (1s) with E_b = 284.5 eV.

The basic properties of the catalysts were determined by CO_2 temperature-programmed desorption (CO_2-TPD). The catalysts (0.1 g, 40–60 mesh) were placed in a quartz reactor bed. After 5 h of pretreatment in Ar flow at 500 °C, the catalysts were cooled to room temperature. Then, they were saturated with pure CO_2 (30 L min^{-1}) using a six-way valve for 3 h and then flushed with Ar (40 L min^{-1}) flow to remove all physically adsorbed molecules. Afterward, the CO_2-TPD experiments were started from 30 to 500 °C with a heating rate of 10 °C min^{-1} under Ar flow (40 L min^{-1}), and the desorbed CO_2 was detected by using an AMETEK mass spectrometer. The CO_2 peak area was quantitatively calibrated by injecting CO_2 pulses.

In situ Fourier transform infrared spectroscopic (FTIR) experiments were performed in a closed stainless FTIR steel cell for scanning at suitable temperatures, and the spectra were recorded with a Nicolet Magna 550 FTIR spectrometer in the region of 4000–400 cm^{-1} at a resolution of 4 cm^{-1}. In the present work, four types of experiments were performed, namely: (a) MC thermal decomposition: 15 mg of MC was ground and pressed to a self-supporting pellet, and then the disk was put into the closed cell. (b) MC adsorption on the catalyst: the sample was obtained by mixing 14 mg of the catalyst and 1 mg of MC, which were then ground and pressed to a self-supporting pellet, and then the pellet was put into the closed cell. (c) Methanol adsorption on the catalyst: 15 mg of the catalyst was finely ground and pressed to a self-supporting pellet. After pretreatment under vacuum for 3 h, 10 μL of methanol was injected into the closed cell. (d) Co-adsorption of MC and methanol on the catalyst: the sample was obtained by mixing 14 mg of the catalyst and 1 mg of MC, which were then ground and pressed to a self-supporting pellet. After pretreatment under vacuum for 3 h, various amounts of methanol (0, 10, 20, 40, 60, 80, and 100 μL) were introduced into the closed cell, and the cell was rapidly heated to 180 °C. Then, the FTIR spectra of co-adsorption of reactants on the catalyst were collected at this temperature. With respect to (a), (b) and (c) experiments, the FTIR cell was heated from room temperature to 200 °C, and the spectra were collected once every 2 min in this work.

2.3 Catalytic test

The catalytic activities of the catalysts for the synthesis of DMC from MC and methanol were evaluated in a 100 mL stainless steel autoclave reactor equipped with electric heating, a reflux column and a magnetic stirrer under the assigned conditions. In a typical process, 0.5 g of the freshly prepared catalysts, 0.05 mol (3.75 g) of MC and 1 mol (32 g) of methanol were placed in the reactor. Then, it was rapidly heated to 200 °C and kept for 6 h with magnetic stirring. During the reaction, the temperature error was less than 2 °C. After the reaction, the autoclave was cooled to room temperature, and the product mixture in the autoclave was weighed, clarified and determined using a gas chromatograph with a PEG-20M capillary column and a flame ionization detector (FID). The column was temperature-programmed from 80 to 180 °C.

3. Results and discussion

3.1 Textural and structural properties of the prepared materials

The XRD patterns of the HTl precursors with $Mg^{2+}:La^{3+}:Al^{3+}$ from 3 : 1 : 0 to 3 : 1 : 1 are shown in Fig. 1(a). Obviously, HT-0La and HT-2La precursors exhibited profiles similar to the pure layered double hydroxide structure with sharp and symmetric peaks for the (003), (006), (110) and (113) planes and broad asymmetric peaks for the (009), (015), and (018) planes (JCPDS 70-2151).[31] For HT-5La, HT-8La and HT-10La samples, the peaks of a mixture of $La(OH)_3$ (JCPDS 06-0585) and $La_2(CO_3)_2(OH)_2$ (JCPDS 70-1774) were also detected.[42–44]

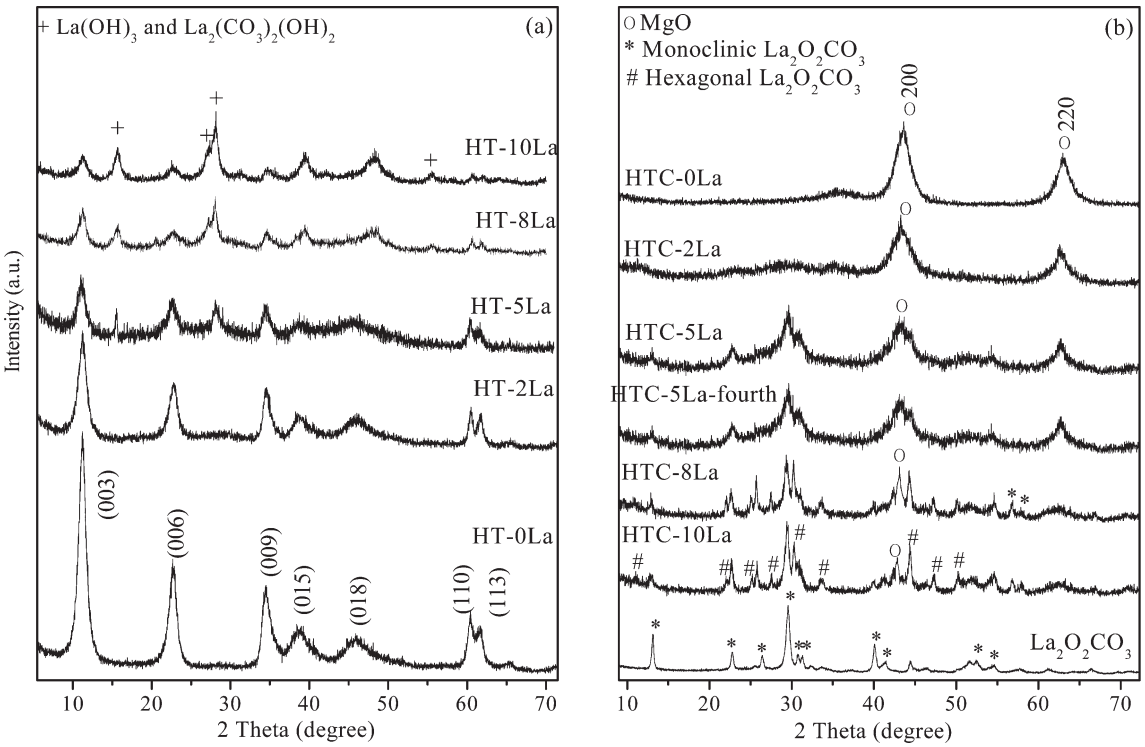

Fig. 1 XRD patterns of HT-La precursors with different La contents (a); HTC-La mixed oxides with different La contents and $La_2O_2CO_3$ catalysts (b).

According to previous reports, La favored the formation of lanthanum carbonate species in the very early stages of the co-precipitation because it possessed the lowest electronegativity compared to other rare earth elements.[42,43,45] Meanwhile, La preferred to be located in the interlayer gallery of HT as separate hydroxide and hydroxyl carbonate phases due to its relatively large ionic radius.[42] On the other hand, the peak intensities and sharpness of the (003) and (006) planes, which were directly proportional to the crystallinity of the material, were observed to decrease with increasing La content of the precursors. This might be ascribed to the following reasons. Firstly, La^{3+} possessed a higher ionic radius (0.103 nm) than Mg^{2+} (0.072 nm) and Al^{3+} (0.053 nm), resulting in large distortions when it was incorporated into the HTl layers. Moreover, it was suggested that a high Al content was favorable for the formation of HTl precursors.[46] In this study, the La^{3+} : Al^{3+} atomic ratios in the starting solution was increased from 0 : 1 to 1 : 1, so the Al content decreased relatively with increasing La content. Consequently, the yields of the HTl phase in the precursors decreased and such an HTl structure almost disappeared when x reached 1.0.

It was well known that HTlcs belonged to the hexagonal crystal system, and they could be described by two important values, a and c.[31] As seen in Table 1, both parameters a and c of La-containing HTl precursors increased with the increase in La content, and the values of these parameters were in good agreement with those reported by others.[42,43] Parameter a ($a = 2d_{110}$) was a function of the average radius of the metal cations in the layers and reflected the density of metal ions

Table 1 Textural and chemical properties as well as weight loss (occurring in the second and third steps of thermal decomposition) of the HTl precursors

Samples	Mg^{2+} : Al^{3+} : La^{3+} atomic ratio[a]	Lattice parameters[b] (Å)		Weight loss (%) (second : third step)	S_{BET} ($m^2\ g^{-1}$)	Pore volume ($cm^3\ g^{-1}$)
		a	c			
HT-0La	3 : 1 : 0	3.061	23.598	18.5 : —	21	0.12
HT-2La	3 : 1 : 0.2	3.063	23.624	13.9 : 7.5	33	0.16
HT-5La	3 : 1 : 0.5	3.066	23.937	12.6 : 8.1	41	0.24
HT-8La	3 : 1 : 0.8	3.068	24.253	12.3 : 9.7	39	0.21
HT-10La	3 : 1 : 1	3.072	24.409	11.9 : .8	36	0.19

[a] The nominal atomic ratio in the synthesis mixture. [b] Determined by XRD, $a = 2d_{110}$, $c = 3d_{003}$.

in the (110) plane. The increase in parameter a might be due to the isomorphous substitution of Mg^{2+} or Al^{3+} by La^{3+} in the HTl layers. La^{3+} exhibited a larger ionic radius in comparison with Mg^{2+} and Al^{3+}; thus more La^{3+} insertion into brucite sheets led to an increase in the average radius of the cations in the layers.[44] Parameter c ($c = 3d_{003}$) was a measure of the thickness of the HTl layer and the interlayer distance, which further relied on the electrostatic force in the HTl interlayer. Due to its larger ionic radius, La^{3+} exhibited a lower charge density than Mg^{2+} and Al^{3+}. Thus, the insertion of La^{3+} into the HTlc layer would cause a decrease in electrostatic forces between the layer and the interlayer. In addition, La^{3+} preferred to be located in the interlayer gallery of HT as separate hydroxide and hydroxyl carbonate phases, which resulted in the decrease of the electrostatic attraction between the layer and interlayer anions, leading to the increase of the layer spacing.[42]

The XRD patterns of the samples after calcination are shown in Fig. 1(b). Clearly, heat treatment of the HTlcs at 500 °C destroyed the HTl structure since no characteristic reflection peaks of HTlcs were found in the XRD patterns. All of these calcined materials presented reflections at 43.3° and 62.8° owing to the (200) and (220) planes, respectively, of the MgO periclase (JCPDS 45-0946) phase. Nevertheless, the intensity of the peaks due to MgO periclase decreased and almost vanished when the La additive amount reached x = 1.0. Diffraction peaks assigned to Al_2O_3 were not found in the calcined catalysts, implying that Al_2O_3 might exist in an amorphous state. As x increased to 0.5, the diffraction peaks ascribed to monoclinic $La_2O_2CO_3$ (JCPDS 48-1113) formed by re-adsorption of gaseous CO_2, coming from HTlc decomposition or air contamination during the sample manipulation, were detected.[42–44] As for HTC-8La and HTC-10La materials, the diffraction peaks of hexagonal $La_2O_2CO_3$ (JCPDS 37-804) also appeared at 2θ of 11.0°, 22.2°, 25.2°, 27.6°, 30.5°, 33.6°, 44.4°, 47.4° and 50.3°, which indicated that a higher content of La was favorable for $La_2O_2CO_3$ crystal transformation from monoclinic to hexagonal. In addition, the formation of $La_2O_2CO_3$ led to the shift of the peaks of the (200) plane of MgO to lower angles, which was probably because of the fact that some La^{3+} ions had been incorporated into the MgO lattice.

Fig. 2 shows the weight loss and the weight loss rates of the HTlcs during calcination, which reveals the transformation of HTl samples into the corresponding mixed oxides. Obviously, the TG profile of the pure Mg–Al hydrotalcite (HT-0La) precursor consisted of two major steps, while the La-containing HTlcs showed four typical weight losses. The first loss for all the samples was associated with the peak at 175–218 °C with a shoulder peak at 67–85 °C. According to previous reports, it was due to the removal of physically absorbed water, interlayer water molecules and small amounts of weakly bound OH groups. The second weight loss at 360–410 °C is due to the elimination of both the hydroxyl groups from the HTl network and carbonate anions from the interlayer anion, resulting in the collapse of the layered structure.[47]

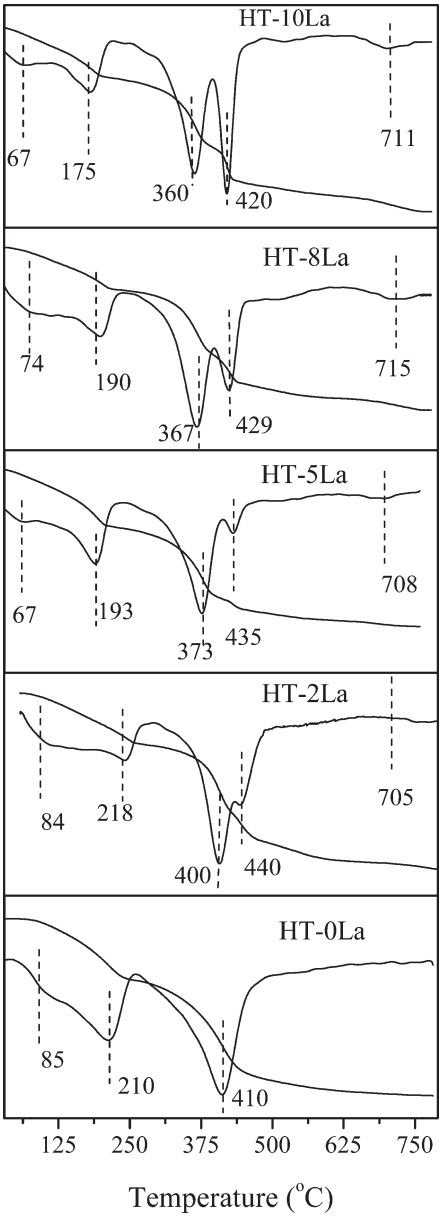

Fig. 2 Thermogravimetry and differential thermogravimetry (TG-DTG) profiles of HTl precursors.

With regard to La-containing precursors, the third weight loss at 420–440 °C might be ascribed to the dehydroxylation of La–OH, resulting in the transformation of La hydroxide and hydroxyl carbonate phases into $La_2O_2CO_3$.[48] Furthermore, another weight loss was found at around 710 °C in La-containing HTlcs, which might be because of the thermal decomposition of $La_2O_2CO_3$.[49] Obviously, this weight loss became more and more intense with increasing La content. This phenomenon was consistent with the result of XRD, which showed that the number of $La_2O_2CO_3$ peaks increased from HTC-2La to HTC-10La samples.

The weight losses for the second and third steps are compared in Table 1. It could be seen that with increasing La content, the second weight loss step due to the

decomposition of the HTl species decreased, while the third weight loss, owing to La hydroxide and hydroxyl carbonate phases, increased. This suggested that the higher the La^{3+}: Al^{3+} atomic ratio in the mother liquor, the less HTl phases and the more separate La hydroxide and hydroxyl carbonate phases existed in the precursors, which was in accordance with the XRD patterns of these samples. In addition, the TG profiles demonstrated that the introduction of La led to a decrease in the decomposition temperatures, especially for the third weight loss in La-containing HTlcs (for example, HT-2La: 440 °C; HT-5La: 435 °C; HT-8La: 429 °C; HT-10La: 420 °C). Furthermore, compared with the HT-0La sample, the second step position in La-containing precursors also shifted toward lower temperature with the increase in La content. These results implied a gradual decrease in the thermal stability of the La-containing HTlcs when x increased from 0.2 to 1.0. It might be ascribed to the presence of separate lanthanum hydroxide and hydroxyl carbonate phases in the interlayer space, which led to a decrease in the electrostatic attraction between the layer and the interlayer anions that resulted in the increase of the interlayer space and lower thermal stability.[42,49]

In the present work, the surface compositions of the calcined samples, as determined by XPS, are compared with the chemical compositions of the catalysts measured by ICP in Table 2. It was clearly observed that the surface was considerably depleted of La, while the same surface was enriched with Mg and Al for La-modified Mg–Al mixed oxides. This was in accordance with the results in a previous report, where La: Zn atomic ratios in the surface decreased significantly when Zn–Al–La HTlcs were prepared.[49]

The textural properties of HTC-La catalysts were determined by the N_2 adsorption–desorption technique. The N_2 adsorption–desorption isotherms and the corresponding pore size distribution of the calcined samples are shown in Fig. 3. Apparently, all the samples showed typical type-IV adsorption isotherms with clear hysteresis loops at higher relative pressure, characteristic of a mesoporous solid, and their pore sizes were widely distributed in the range of 5–45 nm. These hysteresis loops were narrow, indicating that the mesoporous pores were regular. Besides, the hysteresis loops exhibited the features of H3 type (IUPAC classification). It is well known that this type of hysteresis is usually related to materials consisting of plate-shaped particles. This was consistent with the traditional view of these types of mixed oxides derived from HTlcs.[50] The specific surface area and pore volume of the calcined samples are listed in Table 2.

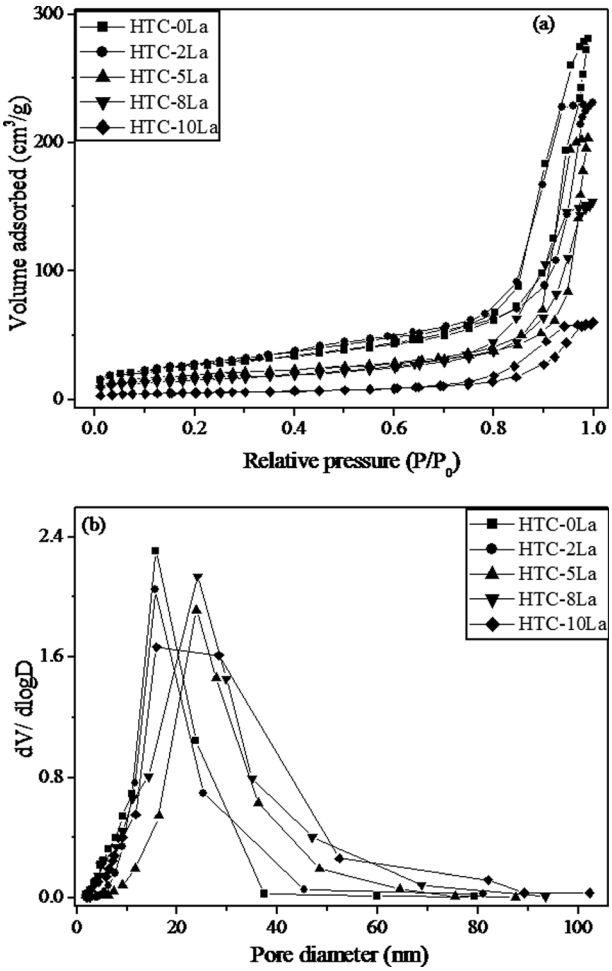

Fig. 3 N_2 adsorption–desorption isotherms (a) and pore-size distributions (b) of HTC-La catalysts.

Table 2 Textural, chemical and basic properties of various catalysts

Sample	S_{BET} ($m^2\ g^{-1}$)	Pore volume ($cm^3\ g^{-1}$)	Atomic ratio in solids[a] $Mg^{2+}:Al^{3+}:La^{3+}$	Surface atomic ratio[b] $Mg^{2+}:Al^{3+}:La^{3+}$	Amounts of basic sites (μmol g^{-1}) and contribution[c] Total	*W*	*M*	*S*
HTC-0La	124	0.33	2.69 : 1 : —	2.47 : 1 : —	193.5	68.1 (35.2)	114.2 (59.0)	11.2 (5.8)
HTC-2La	106	0.52	2.72 : 1 : 0.21	2.41 : 1 : 0.09	223.8	60.6 (27.1)	141.5 (63.2)	21.7 (9.7)
HTC-5La	95	0.49	2.83 : 1 : 0.54	2.64 : 1 : 0.16	264.5	51.8 (19.6)	180.1 (68.1)	32.6 (12.3)
HTC-8La	84	0.45	2.85 : 1 : 0.88	2.66 : 1 : 0.28	242.4	42.0 (17.3)	152.2 (62.8)	48.2 (19.9)
HTC-10La	71	0.41	2.93 : 1 : 1.12	2.75 : 1 : 0.34	211.6	22.0 (10.4)	120.4 (56.9)	69.2 (32.7)
$La_2O_2CO_3$	28	0.16	—	—	107.7	52.6 (48.9)	31.8 (29.5)	23.3 (21.6)

[a] Values measured by ICP. [b] Evaluated by XPS. [c] The value in parentheses was the contribution of single basic sites to the number of total basic sites.

It could be seen that the calcined samples had a higher surface area and pore volume than the corresponding HTls (see Table 1), which could be ascribed to the fact that a large amount of CO_2 was released from HTlcs during calcination.[41] This might be favorable for them to exhibit high catalytic activity. Prescott *et al.* and Meher *et al.* have reported that a high content of Al_2O_3 in the catalysts was favorable to increase the specific surface area.[51,52] Besides, as discovered by Cantrell *et al.*, Al favored higher CO_3^{2-} contents in the interlayer; therefore more open porous networks were formed after thermal treatment.[53] In this work, as the La content increased, correspondingly, the content of Al decreased relatively in these La-containing mixed oxides. At the same time, La might be incorporated into the pore system of HTC-La catalysts during the preparation process. So, their surface area and pore volume became lower as x increased from 0 to 1.0 (see Table 2). Furthermore, the lowest surface area of HTC-10La, which was not favorable for the exposure of more active sites, could also be attributed to the formation of large sintered particles (see the SEM profiles).[49]

The morphologies of the HTl precursors are shown in Fig. 4. All the HTl samples consisted mainly of well-developed and plate-shaped crystals, which suggested the formation of a layered structure. For the pure Mg–Al HT (HT-0La) material, it exhibited mainly hexagonal plate-shaped crystals, which was the same as the result in the previous literature.[38] However, the surface of the plate-shaped crystals became rough and indistinct with the increase in La additive amount. This also implied that the introduction of lanthanum was not favorable for the synthesis of the HTl structure, which was in agreement with the XRD results and previous reports.[42,43,49] The particles of the samples calcined after 500 °C maintained a similar morphology to that of the precursors, though some crystals were destroyed (see Fig. 5). Meanwhile, their particles seemed to be sintered and the particle size of the calcined samples increased as the La additive amount increased. This might be because of the formation

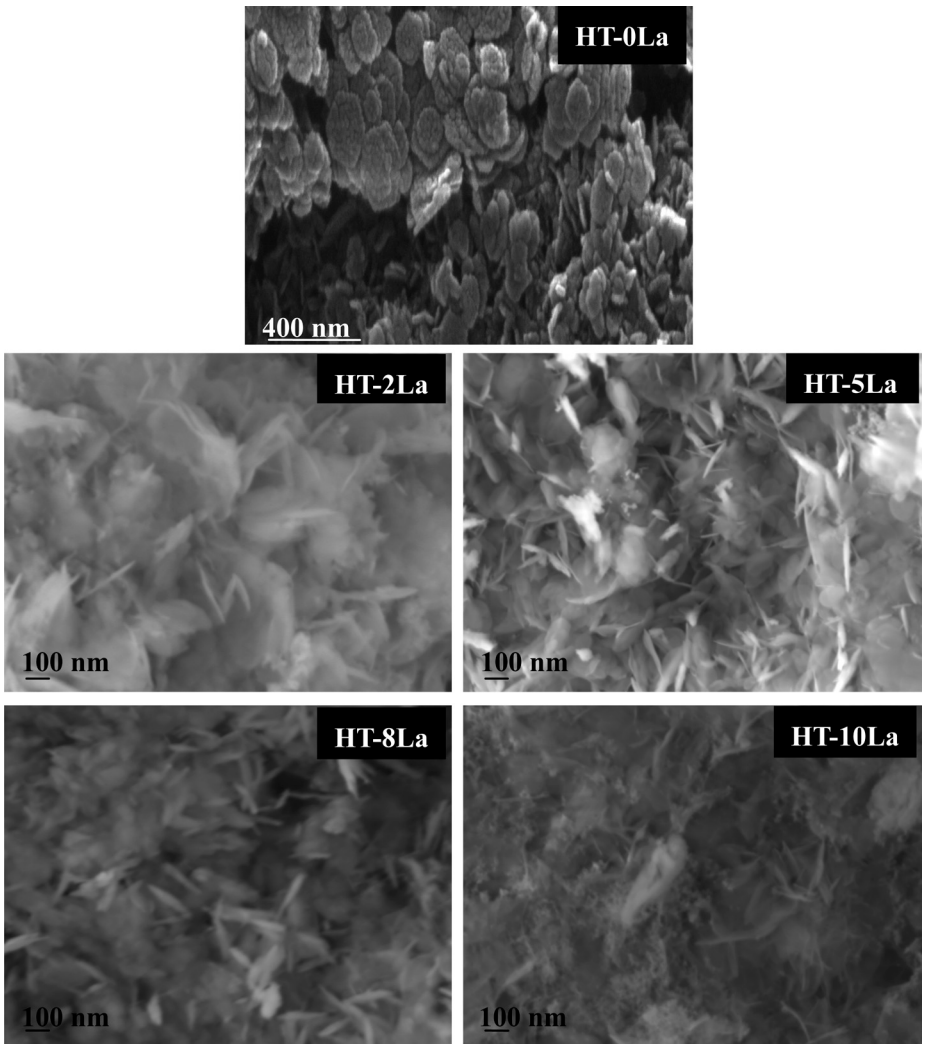

Fig. 4 SEM images of HTl precursors.

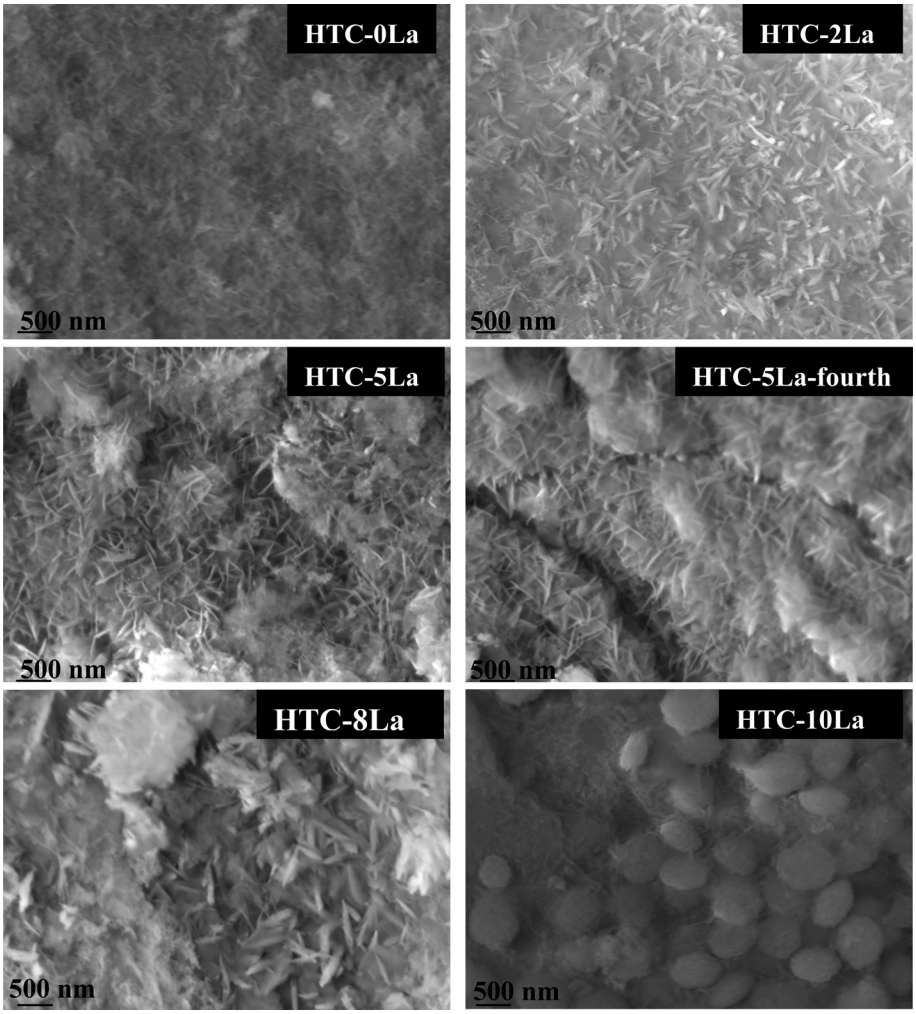

Fig. 5 SEM images of mixed oxides.

the $La_2O_2CO_3$ phase in the catalysts, which was proved by the XRD patterns in Fig. 1(b). Considering that their surface area decreased with the increase in La additive amount, it was reasonable to suggest that less $La_2O_2CO_3$ phase and smaller particle size favor the formation of mixed oxide catalysts with higher specific surface area.

3.2 The surface basicity of catalysts

For solid base catalysts, two factors including basic strength and total basicity (basic site amount per unit weight of catalyst) were selected to evaluate their surface basic properties.[54] Here, the surface basic properties of the catalysts were examined by CO_2-TPD and the basic species could be assigned according to the temperature at which peaks appeared. Higher desorption temperature pointed to stronger basic strength and higher CO_2 uptake indicated higher total basicity. Fig. 6 shows the CO_2 desorption profiles for the prepared La-modified Mg–Al mixed oxides. For comparison, the produced $La_2O_2CO_3$ sample was also investigated. Apparently, the TPD profiles of these samples could be split into three Gaussian peaks, indicating that three types of basic sites with different strengths were present on each surface. Depending on the temperature of desorption, these desorption peaks could be assigned to weak (CO_2 desorption below 200 °C), moderate (CO_2 desorption between 200 and 400 °C) and strong (CO_2 desorption higher than 400 °C) basic sites. According to the description of reported studies, the weak basic sites were related to OH^- groups, the moderate basic sites were associated with metal–oxygen pairs (such as Mg–O, Al–O, and La–O), and the strong basic sites were assigned to low-coordination unsaturated oxygen atoms.[38,41,55] And from the CO_2-TPD profiles of the HTC-La samples, both the moderate and strong basic sites gradually shifted to higher temperature with the rise of La content, which suggested that a greater amount of La content resulted in the increase in moderate and strong basic strength. Moreover, it should be mentioned that among all the samples, $La_2O_2CO_3$ showed the highest desorption temperature of the strong basic sites at about 437 °C. Thus, based on CO_2-TPD characterization, the basic strength of these catalysts followed this order:

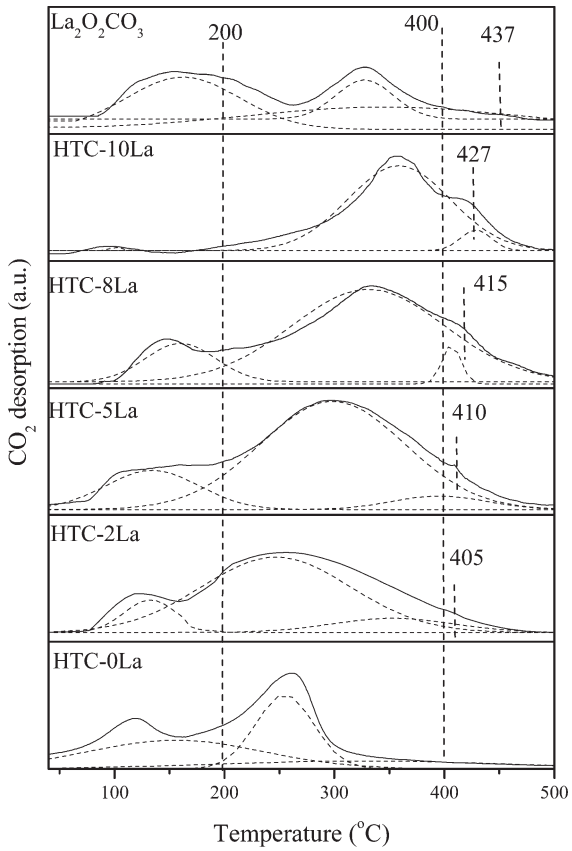

Fig. 6 CO_2-TPD of HTC-La catalysts and $La_2O_2CO_3$ sample.

$La_2O_2CO_3$ > HTC-10La > HTC-8La > HTC-5La > HTC-2La > HTC-0La.

On the other hand, the basicity of all the samples is listed in Table 2. One can see that the $La_2O_2CO_3$ catalyst showed the least total basicity, which might be due to its low specific surface area resulting in the decrease of its exposed basic sites. Moreover, the contribution of the weak basic sites to the total basic sites was about 50%. For the La-containing mixed oxides, this proportion decreased with increasing La additive amount, and their moderate and strong basic peaks were more intense (72.9–89.6% of the total number of basic sites). Therefore, the presence of La not only improved the basic strength, but also promoted the amounts of moderate and strong basic sites of HTC-La catalysts. Notably, although the number of strong basic sites of HTC-La increased as the La content increased, the amount of moderate basic sites increased first and reached the maximum when x was 0.5. Then, it gradually decreased with further increase in La content. These results revealed that apart from the BET surface area, there was some other cause that was responsible for the change in the number of moderate and strong basic sites. In theory, introduction of La could increase the amount of metal–oxygen pairs (La–O) on the catalyst surface, and led to the rise in the number of moderate basic sites for metal oxides. Nevertheless, as reported by Wu *et al.*, the metal–oxygen pairs could partially break up, which led to the generation of coordinatively unsaturated O^{2-} ions, and the lower stability of the layered structure was beneficial to the formation of unsaturated O^{2-} ions.[56] According to the above analysis based on TGA, a gradual decrease in the thermal stability of the La-containing HTlcs was found when x increased from 0 to 1.0. Consequently, the metal–oxygen pairs in the mixed oxides would gradually transform to unsaturated O^{2-} ions as the La content increased. Therefore, it seemed that both the BET surface area and La content could affect the number of basic sites and surface basic site distribution of HTC-La catalysts. Considering the amounts of both moderate and strong basic sites, their basic densities decreased in the following sequence: HTC-5La (212.7 μmol g^{-1}) > HTC-8La (200.4 μmol g^{-1}) > HTC-10La (189.6 μmol g^{-1}) > HTC-2La (163.2 μmol g^{-1}) > HTC-0La (125.4 μmol g^{-1}) > $La_2O_2CO_3$ (55.1 μmol g^{-1}). So, for HTC-La catalysts, the basicity of the moderate and strong basic sites first increased until x = 0.5, then decreased with further increase in La content.

3.3 Catalytic performance

3.3.1 The reaction system of MC and methanol to synthesize DMC. It is well known that the reaction system of MC and methanol could be described by reactions 1–3 in Scheme 1 no matter what catalyst is used.

At first, DMC could be synthesized *via* the substitution of the amino group of MC by the methoxy group in methanol. The product DMC, which was a favorable methylating agent for the amino group, could further react with MC to yield *N*-methyl methyl carbamate (NMMC).[12] Furthermore, at a relatively high reaction temperature, DMC was easily thermally decomposed into dimethyl ether (DME) and carbon dioxide in the presence of solid basic and acidic oxides.[57,58] It should be mentioned that DME could not be detected by GC because it was easily volatilized when the autoclave was opened.[18–24] Thus, the catalysts were evaluated on the basis of MC conversion, DMC yield and selectivity, and NMMC yield in the present case.

3.3.2 Effect of La content on the DMC synthesis. The catalytic performances of various catalysts were evaluated for the methanolysis of MC to DMC. The results are summarized in Table 3. Notably, the reaction of MC and methanol hardly occurred in the absence of a catalyst (entry 1). However, HTC-0La exhibited high activity towards DMC synthesis, yielding 28.2% DMC. The catalytic performances of the La-containing mixed oxide catalysts are presented in entries 3–6. The four catalysts all gave higher MC conversion compared to the HTC-0La sample, indicating that they had higher catalytic activities. Nevertheless, the DMC yield and selectivity differed significantly among them. When the HTC-2La catalyst was used, a 34.7% yield of DMC was achieved, which was a bit higher than that of HTC-0La. Under the same reaction conditions, HTC-5La exhibited excellent catalytic performance with a high DMC yield of 54.3% and a good DMC selectivity of 80.9%. As the La additive amount further increased, both the MC conversion and the DMC selectivity decreased

$$NH_2COOCH_3+CH_3OH \longrightarrow CH_3OCOOCH_3+NH_3 \quad (1)$$

$$NH_2COOCH_3+CH_3OCOOCH_3 \longrightarrow CH_3NHCOOCH_3+CH_3OH+CO_2 \quad (2)$$

$$CH_3OCOOCH_3 \longrightarrow CH_3OCH_3+CO_2 \quad (3)$$

Scheme 1 The reaction system for the reaction of MC and methanol.

Table 3 Catalytic performance of various catalysts in the present work[a]

Entry	Catalyst	MC conversion (%)	DMC selectivity (%)	DMC yield (%)	NMMC yield (%)
1	—	4.1	63.4	2.6	0
2	HTC-0La	32.3	87.3	28.2	1.2
3	HTC-2La	41.2	84.2	34.7	2.0
4	HTC-5La	67.1	80.9	54.3	4.1
5	HTC-8La	59.5	72.6	43.2	5.7
6	HTC-10La	52.4	64.5	33.8	8.9
7	$La_2O_2CO_3$	21.9	51.6	11.3	0.3

[a] Reaction conditions: reaction temperature, 200 °C; reaction time, 6 h; catalyst amount, 0.5 g; MC, 0.05 mol; methanol, 1.0 mol. The product selectivity and yields were based on MC.

remarkably. For instance, HTC-8La and HTC-10La catalysts gave 43.2% and 33.8% DMC yields, respectively. At the same time, their selectivity decreased to 72.6% and 64.5%, respectively. Besides, a further investigation into the performance of the prepared $La_2O_2CO_3$ was also conducted. Obviously, it showed inferior activity compared with the aforementioned mixed oxide catalysts (entry 7). More important, it is noteworthy that for these catalysts, their catalytic activities decreased in the sequence of HTC-5La > HTC-8La > HTC-10La > HTC-2La > HTC-0La > $La_2O_2CO_3$. Meanwhile, the DMC selectivity achieved over them followed this order: HTC-0La > HTC-2La > HTC-5La > HTC-8La > HTC-10La > $La_2O_2CO_3$. So, the current catalytic performance tests suggested that the insertion of La into Mg–Al mixed oxides could remarkably improve the DMC synthesis from MC and methanol.

3.3.3 Effect of basic properties on the DMC synthesis. For catalysts, an increase in their BET surface areas was favorable for achieving higher catalytic activity. The surface areas of the catalysts are listed in Table 2. It could be seen that their BET surface areas decreased in the order of HTC-0La > HTC-2La > HTC-5La > HTC-8La > HTC-10La > $La_2O_2CO_3$. However, their catalytic activity followed this sequence: HTC-5La > HTC-8La > HTC-10La > HTC-2La > HTC-0La > $La_2O_2CO_3$. Thus, the BET surface area of the catalysts was not the sole factor for their catalytic activity in the present work. As mentioned in the discussion above, the moderate and strong basic sites of the HTC-La samples were enhanced remarkably; therefore, their catalytic activities might be closely related to the amounts of moderate and strong basic sites. In addition, it should be noted that the DMC selectivity decreased as the

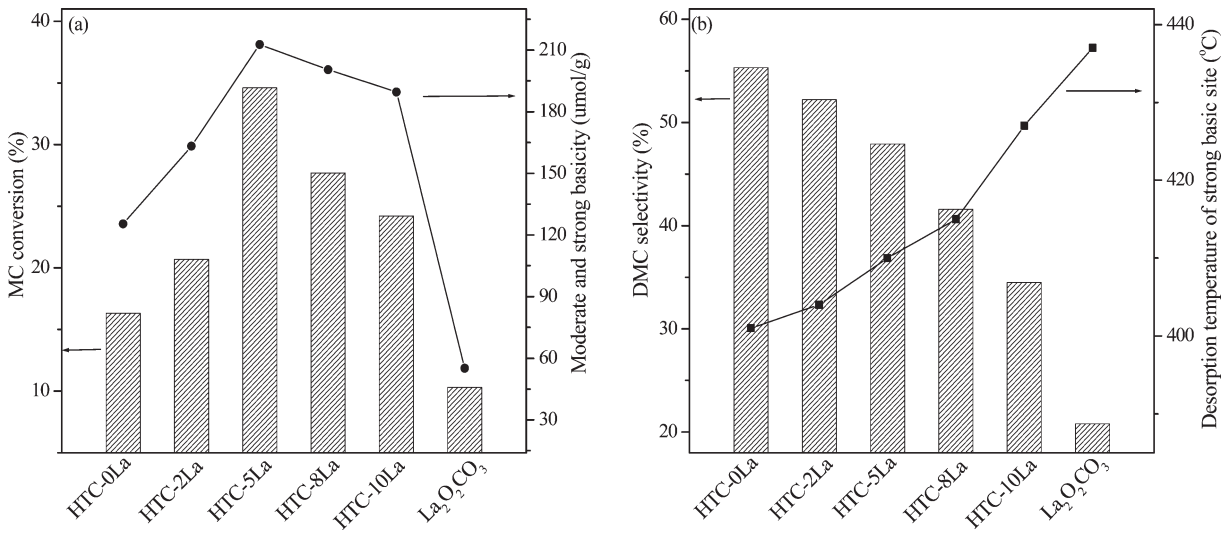

Fig. 7 The correlation between MC conversion and the amounts of both moderate and strong basic sites (a); the relationship between DMC selectivity and desorption temperature of strong basic sites (basic strength) (b).

basic strength of strong basic sites increased. In order to clarify well the correlation between the MC conversion and the amounts of both moderate and strong basic sites, as well as the relationship between their DMC selectivity and basic strength, we illustrated the catalytic performance at 2 h when the reaction was at the beginning in Fig. 7. It could be seen that the sequence of MC conversion was in good agreement with the trend of basicity of both moderate and strong basic sites (Fig. 7(a)), whereas the trend for DMC selectivity was observed to be in contrast with the order of their basic strength (Fig. 7(b)). These phenomena further suggested that the amounts of moderate and strong basic sites played a crucial role in MC conversion. However, a too strong basic strength was not beneficial to obtaining a high DMC selectivity, which might be because of the fact that side reactions such as thermal decomposition of DMC and NMMC synthesis would aggravate over strong basic catalysts.[57,58] This was consistent with the results in previous work, in which the DMC selectivity also decreased with rise of basic strength when basic oxides such as CaO, La_2O_3 and MgO were used as catalysts.[12] Therefore, it was reasonable to draw the conclusion that the enhancement of the catalytic performance of La-modified Mg–Al mixed oxide catalysts towards DMC synthesis from MC and methanol was due to the adjustment of the basic properties by incorporation of a suitable amount of La additive.

3.3.4 Effect of reaction conditions over HTC-5La catalyst. The reaction conditions were further optimized over the HTC-5La catalyst. The effect of reaction temperature on the DMC synthesis is illustrated in Fig. 8(a). Obviously, the reaction temperature exhibited a significant impact on the reaction. The conversion of MC consistently increased with the increase in temperature. However, the DMC yield and selectivity increased sharply in the temperature range of 180–200 °C, and then decreased when the reaction temperature exceeded 200 °C. It could be seen that the maximum DMC yield of 54.3% with the highest DMC selectivity of 80.9% was obtained when the reaction temperature was 200 °C. Theoretically, the DMC synthesis was an endothermic reaction and the temperature had a positive effect on DMC formation.[19] However, higher temperature also shortened the time needed to reach the maximum DMC concentration and accelerated the rate of side reactions including *N*-methylation of MC. As a result, the yield of the by-product NMMC increased significantly to 6.4% at the cost of DMC consumption when the reaction temperature was 210 °C. Therefore, the suitable reaction temperature should be 200 °C.

The effect of reaction time on the DMC synthesis is demonstrated in Fig. 8(b). Clearly, as the reaction proceeded, the conversion of MC increased. The DMC yield and selectivity reached their maximal values at 6 h, and then, the consumption of DMC in the further reaction surpassed gradually the

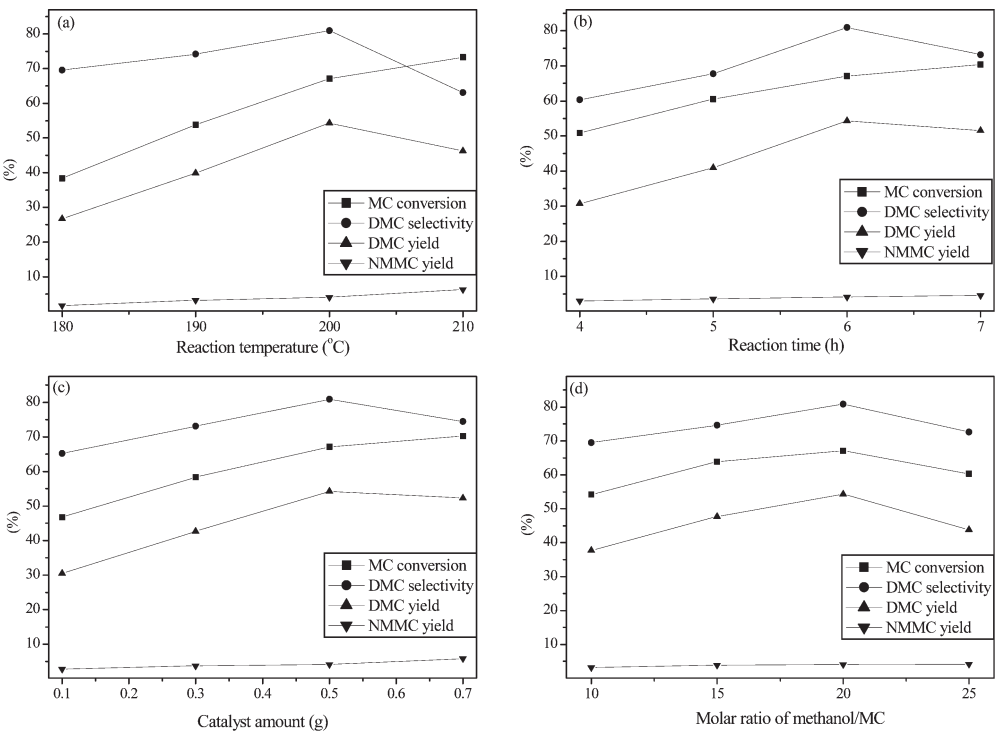

Fig. 8 Effect of reaction conditions on the DMC synthesis over the HTC-5La catalyst. Effect of reaction temperature (a). Reaction conditions: reaction time, 6 h; catalyst amount, 0.5 g; molar ratio of methanol/MC, 20 : 1. Effect of reaction time (b). Reaction conditions: reaction temperature, 200 °C; catalyst amount, 0.5 g; molar ratio of methanol/MC, 20 : 1. Effect of catalyst amount (c). Reaction conditions: reaction temperature, 200 °C; reaction time, 6 h; molar ratio of methanol/MC, 20 : 1. Effect of the molar ratio of methanol/MC (d). Reaction conditions: reaction temperature, 200 °C; reaction time, 6 h; catalyst amount, 0.5 g.

formation of DMC from MC. Thus, the suitable reaction time was chosen as 6 h.

The effect of the catalyst amount was also studied and the results are shown in Fig. 8(c). With the increase of the catalyst amount, the conversion of MC always monotonically increased, but the DMC yield and selectivity reached the maximum values of 54.3% and 80.9% at 0.5 g and then decreased. It was ascribed to the fact that the yield of further reaction product NMMC increased gradually when the catalyst amount was more than 0.5 g. Therefore, the suitable catalyst amount was chosen as 0.5 g in the present case.

The effect of the methanol/MC molar ratio on DMC synthesis is presented in Fig. 8(d). The results demonstrate clearly that the DMC yield and selectivity increased first in the range of 10–20 and then decreased in the range of 20–25. When the methanol/MC molar ratio was 20, the DMC yield and selectivity reached the maximum 54.3% and 80.9%, respectively. When the methanol/MC molar ratio was lower than 20, the MC concentration was higher and the side reaction of *N*-methylation of MC with DMC would occur easily, resulting in a lower DMC yield and selectivity. In theory, a higher methanol/MC molar ratio could promote the reaction equilibrium towards DMC synthesis. Nevertheless, a too high methanol/MC molar ratio would lead to the reduction of MC concentration. Besides, the following *in situ* FTIR experiments revealed that MC and methanol molecules were co-absorbed on the surface basic sites of the HTC-5La catalyst. Consequently, some active sites of the catalyst for activating MC would be occupied by a larger amount of methanol. Thus, the reaction rate might decrease, resulting in a lower DMC yield when the methanol/MC molar ratio exceeded 20. In the present case, from a practical view, the suitable methanol/MC molar ratio was selected as 20.

3.3.5 Reusability and stability of HTC-5La catalyst. The reusability of catalysts played a crucial role in the DMC synthesis *via* MC methanolysis in practical industrial production. Therefore, in order to explore a highly effective and stable solid catalyst, the reusability of HTC-5La was also investigated. After the first run, the used HTC-5La sample was separated by filtration, washed with methanol several times, dried in an oven at 80 °C and reused without any pretreatment. Its catalytic performance was evaluated and the results are shown in Fig. 9. To our delight, HTC-5La could be recycled and reused at least four times without obvious loss of activity. At the same time, the recovered HTC-5La catalyst after reused four times (HTC-5La-fourth) was analyzed using SEM and XRD techniques. SEM presented that the plate-like morphology was unchanged after the catalyst was used four times (see Fig. 5). Additionally, the XRD pattern of HTC-5La-fourth is shown in Fig. 1(b). Obviously, its diffraction peak number was the same as the fresh one, and the peak intensity didn't show any significant change. Therefore, the HTC-5La catalyst exhibited higher stability than previously reported zinc-based catalysts for this reaction, and a heterogeneous solid catalyst with excellent catalytic performance and stability was successfully developed.

3.4 FTIR spectra between reactants and HTC-5La catalyst

The adsorption behaviours on the solid catalyst surface play an important role in the reaction pathways. In order to

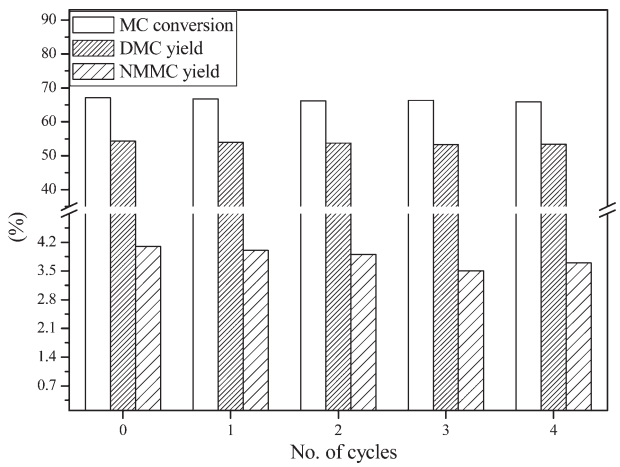

Fig. 9 Reusability of the HTC-5La catalyst for the DMC synthesis from MC and methanol. Reaction conditions: 200 °C, 6 h, 0.5 g of catalyst, 0.05 mol of MC, 1.0 mol of methanol.

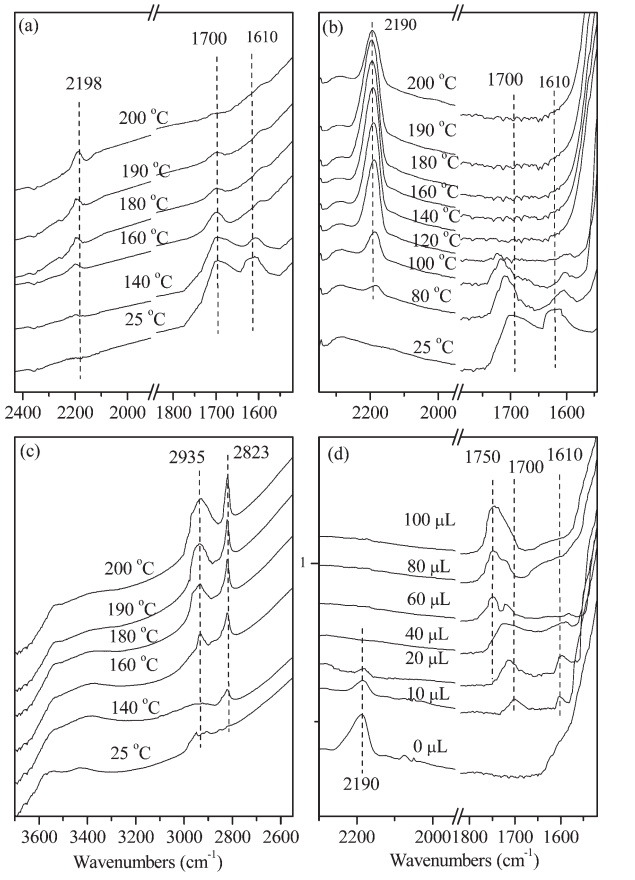

Fig. 10 FTIR spectra evolution of MC (a); MC absorbed on HTC-5La (b); methanol absorbed on HTC-5La (c) at different temperatures; and MC with various amounts of methanol co-adsorbed on HTC-5La at 180 °C (d).

investigate the possible mechanism of the reaction between MC and methanol, *in situ* FTIR experiments under different conditions were conducted.

3.4.1 MC decomposition. Fig. 10(a) demonstrates the FTIR spectra evolution of MC with increasing temperature. At room temperature, the characteristic bands of MC ascribed to the C═O stretching vibration (amide I band) and NH_2 bending vibration (amide II band) were observed at 1700 and 1610 cm^{-1}, respectively.[59] It is worth noting that a new band appeared at 2198 cm^{-1}, which was assigned to the N═C═O asymmetric stretching vibration of isocyanic acid when the temperature surpassed 140 °C.[17,60] Apparently, the intensity of the bands attributed to MC decreased, accompanying that of the band at 2198 cm^{-1} that increased rapidly with further increase in temperature. This implied that the formation of isocyanic acid was due to the decomposition of MC, which was in accordance with the results discovered by Li *et al.*[60]

3.4.2 MC adsorption on HTC-5La catalyst. Then, the adsorption of MC over the HTC-5La catalyst was studied at given temperature regions, and the FTIR spectra are shown in Fig. 10(b). Clearly, the intensity of both amide I and amide II bands of MC decreased rapidly as the temperature increased. At the same time, the amide I band showed a blue shift gradually from 1700 to 1728 cm^{-1}, accompanying the red shift of the amide II band from 1610 to 1598 cm^{-1} before it disappeared, which did not occur when pure MC decomposed. These alternations pointed out the interaction of nitrogen in MC with unsaturated metal cation sites on the HTC-5La catalyst, resulting in the amino group of MC bound to the metal oxide surface (M–NH_2).[61] More important, a new band assigned to the stretching vibration of N═C═O bound to the metal oxide surface (M–N═C═O, M═Mg, Al or La) was found at around 2190 cm^{-1}. It could be seen that the intensity of N═C═O increased first before the temperature increased to 160 °C, implying that MC was swiftly activated and decomposed into isocyanic acid over the catalyst. However, its intensity decreased with further increase in temperature, suggesting the enhanced desorption of isocyanate-containing species. In addition, compared to the blank test without the catalyst, the characteristic band of N═C═O was clearly observed at a lower temperature of 80 °C on the HTC-5La catalyst surface. Thus, all these results proved that MC could be activated over the HTC-5La catalyst and the characteristic band of N═C═O still existed when the temperature increased to 200 °C.

3.4.3 Methanol adsorption on HTC-5La catalyst. Fig. 10(c) illustrates the FTIR spectra evolution of methanol adsorbed on the HTC-5La catalyst at different temperatures. Two new bands at 2395 and 2823 cm^{-1} corresponding to C–H asymmetric and symmetrical stretching vibrations of deprotonated methanol or methoxide species were clearly visible, which indicated the adsorption of the methoxy group on the surface of the HTC-5La catalyst. This was in accordance with previously reported studies of adsorbed methanol on metal oxide catalysts.[22,62] Thus, these experimental results suggested that methanol could be activated and deprotonated over the HTC-5La catalyst, resulting in the formation of methoxide species coordinated to metal atoms. Moreover, the two bands became more and more obvious at higher temperature, implying that methanol was prone to deprotonation, forming methoxy groups on the catalyst surface at higher temperature.

3.4.4 Co-adsorption of MC and methanol on HTC-5La catalyst. In order to study the reaction procedure on the HTC-5La catalyst more clearly, we carried out MC and methanol co-adsorption experiments (see Fig. 10(d)). In the present case, we followed the change of the band at 2190 cm^{-1} corresponding to the stretching vibration of N═C═O bound to the metal oxide surface (M–N═C═O), the band at 1750 cm^{-1} assigned to the C═O stretching vibration of DMC,[63] as well as the amide I and II bands of MC. Without methanol, MC was activated and decomposed into isocyanic acid species by the basic sites of the catalyst. As the amount of methanol increased, the intensity of M–N═C═O decreased quickly and disappeared when the amount of methanol increased to 40 μL. During this process, the characteristic bands of MC were found at about 1700 and 1610 cm^{-1}. This revealed that the decomposition of MC might be a reversible reaction, and MC would be re-generated *via* the reaction between methanol and isocyanic acid species when excessive methanol existed in the reaction system. At the same time, it should be noted that for the MC molecule, its amide I band had a blue shift, while the amide II band showed a red shift before they disappeared. This also implied that MC was adsorbed on the catalyst surface and its amino group was coordinated with the cationic metal surface atom (M–NH_2).[61] Besides, a new band at 1750 cm^{-1} ascribed to DMC was detected when the methanol amount was 60 μL. Apparently, the amide I and II bands of MC decreased rapidly with the further increase in methanol amount, and they vanished as the amount of methanol reached 100 μL. Meanwhile, the intensity of the characteristic band of DMC consistently increased during this process, revealing the production of DMC from MC and methanol over the HTC-5La catalyst.

3.4.5 Plausible reaction mechanism for DMC synthesis from MC and methanol. According to the FTIR experimental results and previous work,[60] a plausible basic catalytic mechanism wherein MC and methanol were activated simultaneously on the surface basic sites of the HTC-5La catalyst was proposed. As shown in Scheme 2, MC was adsorbed on the catalyst surface through its amino group bound to the metal oxide surface. Consequently, MC was easily decomposed into isocyanic acid. As mentioned in the discussion above, the decomposition of MC into isocyanic acid and methanol might be a reversible reaction. In this work, because the molar ratio of methanol/MC was selected as 20, the reaction equilibrium would shift to MC formation in the presence of excessive methanol in a short time. Then, the re-synthesized MC was coordinated with the cationic surface metal (Mg, Al or La) atom of the mixed oxide through the N atom of the amino group. As a result, the electrons of the C–N group of MC would be redistributed, and then, the

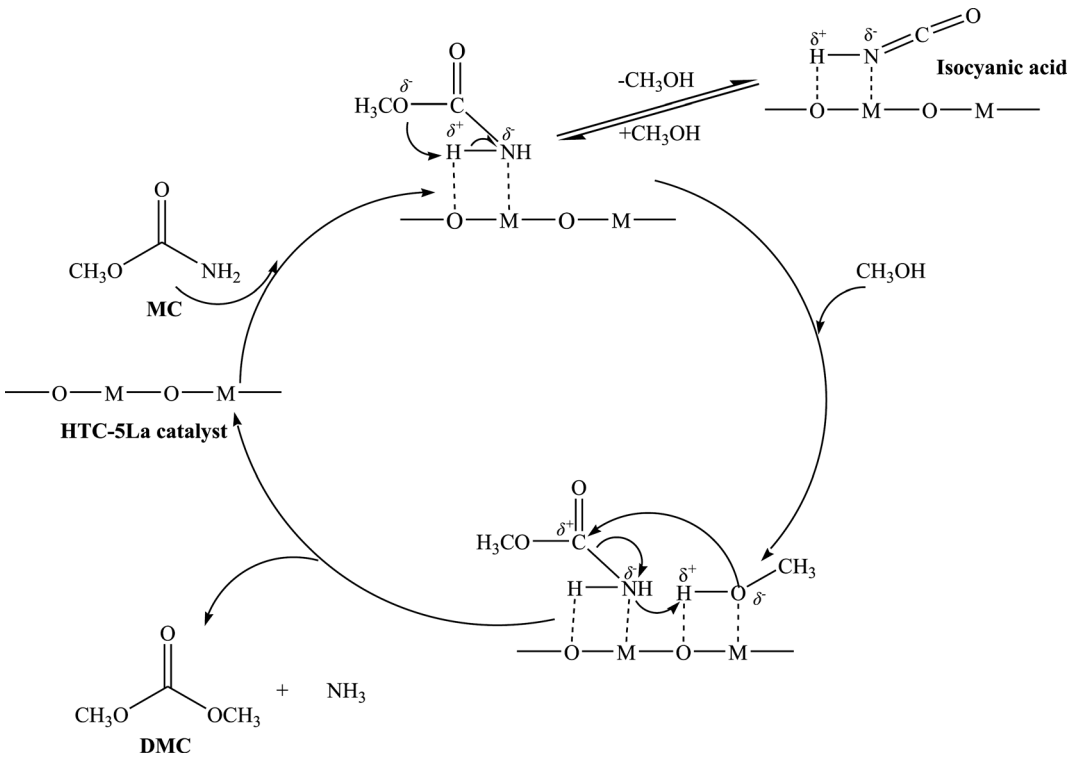

Scheme 2 Possible reaction mechanism for the DMC synthesis from MC and methanol over HTC-5La catalyst.

proton moved to the carbon atom with the appearance of a carbocation and a nitrogen anion. At the same time, the HTC-5La catalyst could also activate methanol through the abstraction of $H^{\delta+}$ by the basic sites, giving a strong nucleophilic methoxy group, which formed a complex with the unsaturated metal cations of the catalyst. Subsequently, a lone pair of electrons of the oxygen atom in the methoxy group formed a bond with the electrophilic carbonyl carbon of the activated MC to generate DMC, while the hydrogen proton breaking away from the methanol molecule combined with the amino group leaving from the activated MC molecule to form NH_3.

3.5 Activity comparison of HTC-5La catalyst with other reference catalysts

In this work, the catalytic activity of the HTC-5La catalyst is compared with several representative catalysts, and the comparative results are listed in Table S1 in the ESI.† Homogeneous catalysts such as $ZnCl_2$ and $LaCl_3$ exhibited good catalytic performance,[28,29] but they were inconvenient for catalyst recovery in practical production. Although ZnO exhibited high catalytic activity towards the reaction between urea and methanol,[19] it was almost inactive for this reaction.[24] In fact, it was a precursor of the homogeneous catalyst for the reaction of urea and methanol.[24] Compared to pure oxide CaO,[12] Fe_2O_3 supported on MCM-49 (Fe_2O_3/HMCM-49) showed higher catalytic activity with 97.3% DMC selectivity.[18] Unfortunately, the DMC yield was lower than 35%. Besides, Zn/Al,[22] Zn/Fe,[30] and ZnO–CeO_2–La_2O_3 mixed oxides[23] were often used to catalyze the DMC synthesis. Even though these catalysts were highly active, their reusability might be limited. The present HTC-5La catalyst showed higher activity compared to the other reported solid catalysts. In addition, the present catalyst was reusable, and its preparation method was simple and repeatable. Based on the above results, we can conclude that the HTC-5La sample is an active, stable and practical catalyst for the DMC synthesis from MC and methanol.

4. Conclusions

La-modified mesoporous Mg–Al mixed oxides derived from hydrotalcite-like compounds containing La (Mg^{2+}:Al^{3+} = 3) with La^{3+}:Al^{3+} varying from 0 to 1.0 were synthesized *via* a simple co-precipitation method followed by hydrothermal treatment. The La content had a significant influence on the physicochemical and catalytic properties of the HTC-La catalysts for the synthesis of DMC from MC and methanol. The following conclusions might be drawn:

(1) The pure and crystalline Mg–Al–La hydrotalcite-like compounds could be obtained by adding suitable amounts of La into pure Mg–Al hydrotalcite, and the yields of hydrotalcite-like compounds decreased with increasing La content.

(2) La could be used to fine-tune the structural, textural and chemical properties of the pure Mg–Al mixed oxides. With the increased La^{3+}:Al^{3+} atomic ratio, the basic strength

of HTC-La monotonically increased. However, the basicity of moderate and strong basic sites first increased until La^{3+}: Al^{3+} = 0.5, then decreased with further increase in La content.

(3) Both the basic strength and basicity of the HTC-La catalysts were demonstrated to have a significant impact on the DMC synthesis. It was found that the catalysts that possessed more moderate and strong basic sites could give high MC conversion. In contrast, the DMC selectivity decreased as the basic strength increased. A suitable amount of La was favorable for the DMC synthesis, and an excellent DMC yield of 54.3% with a high DMC selectivity of 80.9% could be achieved over the HTC-5La catalyst. Simultaneously, this catalyst exhibited high stability on the basis of the reusability test and SEM, XRD and N_2 adsorption–desorption characterization.

(4) The *in situ* FTIR experiments revealed that MC and methanol were co-adsorbed on the surface of the HTC-5La sample. Further study indicated that MC was decomposed into a metal isocyanato group, and methanol was activated to produce a strong nucleophilic methoxy group by the basic sites. Finally, a plausible basic catalytic mechanism was proposed for this catalytic reaction.

Acknowledgements

This work is financially supported by the "Strategic Priority Research Program—Climate Change: Carbon Budget and Related Issues" of the Chinese Academy of Sciences (XDA05010108), the National Natural Science Foundation of China (21401164), the Natural Science Foundation of Shandong Province, China (ZR2012BL07, ZR2013BL019), and the State Key Laboratory of Coal Conversion Open Foundation (J12-13-609).

Notes and references

1 Y. Ono, *Appl. Catal., A*, 1997, **155**, 133–166.
2 A. Dibenedetto and A. Angelini, *Adv. Inorg. Chem.*, 2014, **66**, 25–81.
3 P. Rounce, A. Tsolakis, P. Leung and A. York, *Energy Fuels*, 2010, **24**, 4812–4819.
4 S. Megahed and W. Ebner, *J. Power Sources*, 1995, **54**, 155–162.
5 H. Hood and H. R. Mordock, *J. Phys. Chem.*, 1919, **23**, 498–512.
6 Sh. Wang, L. Wei, Y. Dong, Y. Zhao and X. Ma, *Catal. Commun.*, 2015, **72**, 43–48.
7 P. Kumar, V. C. Srivastava and I. M. Mishra, *Catal. Commun.*, 2015, **60**, 27–31.
8 B. A. Santos, V. M. Silva, J. M. Loureiro and A. E. Rodrigues, *ChemBioEng Rev.*, 2014, **1**, 214–229.
9 M. Zhang, M. Xiao, Sh. Wang, D. Han, Y. Lu and Y. Meng, *J. Cleaner Prod.*, 2015, **103**, 847–853.
10 D. C. Stoian, E. Taboada, J. Llorca, E. Molins, F. Medina and A. M. Segarra, *Chem. Commun.*, 2013, **49**, 5489–5491.
11 P. Ball, H. Fuellmann and W. Heitz, *Angew. Chem., Int. Ed. Engl.*, 1980, **19**, 718–720.
12 M. H. Wang, H. Wang, N. Zhao, W. Wei and Y. H. Sun, *Catal. Commun.*, 2006, **7**, 6–10.
13 J. J. Sun, B. L. Yang and H. Y. Lin, *Chem. Eng. Technol.*, 2004, **27**, 435–439.
14 T. Cho, T. Tamura, T. Cho and K. Suzuki, *US Pat.*, 5534649, 1996.
15 B. L. Yang, D. P. Wang, H. Y. Lin, J. J. Sun and X. P. Wang, *Catal. Commun.*, 2006, **7**, 472–477.
16 H. Wang, B. Lu, X. G. Wang, J. W. Zhang and Q. H. Cai, *Fuel Process. Technol.*, 2009, **90**, 1198–1201.
17 Q. B. Li, N. Zhao, W. Wei and Y. H. Sun, *J. Mol. Catal. A: Chem.*, 2007, **270**, 44–49.
18 Ch. Zhang, B. Lu, X. G. Wang, J. X. Zhao and Q. H. Cai, *Catal. Sci. Technol.*, 2012, **2**, 305–309.
19 M. H. Wang, N. Zhao, W. Wei and Y. H. Sun, *Ind. Eng. Chem. Res.*, 2005, **44**, 7596–7599.
20 W. Joe, H. J. Lee, U. G. Hong, Y. S. Ahn, C. J. Song, R. J. Lwon and I. K. Song, *J. Ind. Eng. Chem.*, 2012, **18**, 1018–1022.
21 X. M. Wu, M. Kang, N. Zhao, W. Wei and Y. H. Sun, *Catal. Commun.*, 2014, **46**, 46–50.
22 X. M. Wu, M. Kang, Y. L. Yin, F. Wang, N. Zhao, F. K. Xiao, W. Wei and Y. H. Sun, *Appl. Catal., A*, 2014, **473**, 13–20.
23 W. Joe, H. J. Lee, U. G. Hong, Y. S. Ahn, C. J. Song, R. J. Lwon and I. K. Song, *J. Ind. Eng. Chem.*, 2012, **18**, 1730–1735.
24 W. B. Zhao, W. C. Peng, D. F. Wang, N. Zhao, J. P. Li, F. K. Xiao, W. Wei and Y. H. Sun, *Catal. Commun.*, 2009, **10**, 655–658.
25 H. An, X. Zhao, L. Guo, C. Jia, B. Yuan and Y. Wang, *Appl. Catal., A*, 2012, **433–434**, 229–235.
26 S. Fujita, Y. Yamanishi and M. Arai, *J. Catal.*, 2013, **297**, 137–141.
27 W. B. Zhao, X. Y. Qin, Y. H. Li, Z. S. Zhang and W. Wei, *Ind. Eng. Chem. Res.*, 2012, **51**, 16580–16589.
28 W. B. Zhao, F. Wang, W. C. Peng, N. Zhao, J. P. Li, F. K. Xiao, W. Wei and Y. H. Sun, *Ind. Eng. Chem. Res.*, 2008, **47**, 5913–5917.
29 D. F. Wang, X. L. Zhang, Y. Y. Gao, F. K. Xiao, W. Wei and Y. H. Sun, *Fuel Process. Technol.*, 2010, **91**, 1081–1086.
30 D. F. Wang, X. L. Zhang, Y. Y. Gao, F. K. Xiao, W. Wei and Y. H. Sun, *Catal. Commun.*, 2010, **11**, 430–433.
31 F. Cavani, F. Trifirò and A. Vaccari, *Catal. Today*, 1991, **11**, 173–301.
32 L. H. Zhang, C. Zheng, F. Li, D. G. Evans and X. Duan, *J. Mater. Sci.*, 2008, **43**, 237–243.
33 P. Gao, F. Li, H. J. Zhan, N. Zhao, F. K. Xiao, W. Wei, L. S. Zhong, H. Wang and Y. H. Sun, *J. Catal.*, 2013, **298**, 51–60.
34 G. Busca, U. Costantino, F. Marmottini, T. Montanari, P. Patrono, F. Pinzari and G. Ramis, *Appl. Catal., A*, 2006, **310**, 70–78.
35 L. Faba, E. Díaz and S. Ordóñez, *Appl. Catal., B*, 2012, **113–114**, 201–211.
36 D. Tichit, D. Lutic, B. Coq, R. Durand and R. Teissier, *J. Catal.*, 2003, **219**, 167–175.
37 M. Mokhtar, T. S. Saleh and S. N. Basahel, *J. Mol. Catal. A: Chem.*, 2012, **353–354**, 122–131.

38 P. Liu, M. Derchi and E. J. M. Hensen, *Appl. Catal., B*, 2014, **144**, 135–143.
39 D. F. Wang, X. L. Zhang, W. Wei and Y. H. Sun, *Catal. Commun.*, 2012, **28**, 159–162.
40 D. F. Wang, X. L. Zhang, Ch. L. Liu, T. T. Cheng, W. Wei and Y. H. Sun, *Appl. Catal., A*, 2015, **505**, 478–486.
41 G. D. Wu, X. Wang, B. Chen, J. P. Li, N. Zhao, W. Wei and Y. H. Sun, *Appl. Catal., A*, 2007, **329**, 106–111.
42 P. Unnikrishnan and D. Srinivas, *Ind. Eng. Chem. Res.*, 2012, **51**, 6356–6363.
43 R. Bîrjega, O. D. Pavel, G. Costentin, M. Che and E. Angelescu, *Appl. Catal., A*, 2005, **288**, 185–193.
44 E. Rodrigues, P. Pereira, T. Martins, F. Vargas, T. Scheller, J. Correa, J. Del Nero, S. G. C. Moreira, W. Ertel-Ingrisch, C. P. D. Campos and A. Gigler, *Mater. Lett.*, 2012, **78**, 195–198.
45 R. D. Shannon, *Acta Crystallogr., Sect. A: Cryst. Phys., Diffr., Theor. Gen. Crystallogr.*, 1976, **32**, 751–767.
46 M. Behrens, I. Kasatkin, S. Kuhl and G. Weinberg, *Chem. Mater.*, 2010, **22**, 386–397.
47 W. Yang, Y. Kim, P. K. T. Liu, M. Sahimi and T. T. Tsotsis, *Chem. Eng. Sci.*, 2002, **57**, 2945–2953.
48 J. P. Ramirez, J. Overeijnder, F. Kapteijin and J. A. Moulijn, *Appl. Catal., B*, 1999, **23**, 59–72.
49 H. G. Li, X. Jiao, L. Li, N. Zhao, F. K. Xiao, W. Wei, Y. H. Sun and B. Sh. Zhang, *Catal. Sci. Technol.*, 2015, **5**, 989–1005.
50 Q. X. Ma, T. Sh. Zhao, D. Wang, W. Q. Niu, P. Lv and N. Tsubaki, *Appl. Catal., A*, 2013, **464–465**, 142–148.
51 H. A. Prescott, Z. Li, E. Kemnitz, A. Trunschke, J. Deutsch, H. Lieske and A. Auroux, *J. Catal.*, 2005, **234**, 119–130.
52 L. C. Meher, R. Gopinath, S. N. Naik and A. K. Dalai, *Ind. Eng. Chem. Res.*, 2009, **48**, 1840–1846.
53 D. G. Cantrell, L. J. Gillie, A. F. Lee and K. Wilson, *Appl. Catal., A*, 2005, **287**, 183–190.
54 K. Tanabe, M. Misono, Y. Ono and H. Hattori, *New solid acids and bases studies in the surface science and catalysis*, Elsevier, Amsterdam, 1989, pp. 14–16.
55 Z. Liu, J. A. Cortés-Concepción, M. Mustian and M. D. Amiridis, *Appl. Catal., A*, 2006, **302**, 232–236.
56 G. D. Wu, X. L. Wang, W. Wei and Y. H. Sun, *Appl. Catal., A*, 2010, **377**, 107–113.
57 Y. Ch. Fu, H. Y. Zhu and J. Y. Shen, *Thermochim. Acta*, 2005, **434**, 88–92.
58 M. Selva, M. Fabris and A. Perosa, *Green Chem.*, 2011, **13**, 863–872.
59 J. C. Carter and J. E. Devia, *Spectrochim. Acta, Part A*, 1973, **29**, 623–632.
60 F. J. Li, H. Q. Li, L. G. Wang, P. He and Y. Cao, *Catal. Sci. Technol.*, 2015, **5**, 1021–1034.
61 S. K. Sahni, *Transition Met. Chem.*, 1979, **4**, 73–76.
62 W. Zhang, H. Wang, W. Wei and Y. H. Sun, *J. Mol. Catal. A: Chem.*, 2005, **231**, 83–88.
63 T. Beutel, *J. Chem. Soc., Faraday Trans.*, 1998, **94**, 985–993.

